Correlation between the composition-dependent properties and phase stability of Co_2YGa (Y = Cr, V) shape-memory alloys from first-principles study

Chun-Mei Li,* Yang Zhang, Wen-Jiang Feng, Ren-Zhong Huang, and Ming Gao
College of Physics Science and Technology, Shenyang Normal University, 253 Huanghe North Street, Shenyang 110034, China

(Received 3 November 2019; revised manuscript received 1 January 2020; accepted 3 February 2020; published 12 February 2020)

The composition-dependent properties and phase stability of Co_2YGa (Y = Cr, V)-based shape-memory alloys are investigated by using the first-principles exact muffin-tin-orbital method in combination with the coherent potential approximation. It is shown that both Co_2CrGa and Co_2VGa alloys possess $L2_1$ structures at the ferromagnetic (FM) state but tetragonal structures at the paramagnetic (PM) state. In off-stoichiometric Co_2YGa alloys, the excess Ga atom has a strong tendency to take the Y sublattice, whereas the excess Co atom tends to take the Y site in the FM $L2_1$ phase when Y = Cr but the Ga site in the other phases when Y = V. The off-stoichiometric Cr78 and Cr79 alloys can occur in the normal martensitic transformation (MT) at the PM state but the reentrant martensitic transformation (RMT) at the FM state, whereas only the normal MT is obtained in the V50 and V15 alloys, where the small difference of the magnetization between the austenite and martensite is supposed to suppress the RMT. In all four groups of off-stoichiometric alloys, the correlation between the composition-dependent properties with the experimental T_M values for the normal MT has been established. In the Cr78 and Cr79 alloys, T_M for the RMT is also predicted to decrease with increasing e/a. The PM ordering tends to soften the elastic constants of all these $L2_1$ alloys. In the four groups of FM $L2_1$ alloys, C', G, E, Θ, and G/B decrease whereas A increases with increasing e/a, which favors T_M for their RMT decreasing but that for their normal MT increasing with e/a. The composition dependence of the MT of these alloys could be explained from their minority density of states around the Fermi level of the $L2_1$ phase by means of the Jahn-Teller effect.

DOI: 10.1103/PhysRevB.101.054106

I. INTRODUCTION

Apart from non-half-metallic Co_2NbSn [1] and Co-Ni-Ga [2], several Co_2-based Heusler alloys have been recently found to possess reversible martensitic transformation (MT) from the $L2_1$ cubic austenite to the $D0_{22}$ tetragonal martensite [3], such as $Co_2Cr(Ga, Si)$ [4], $Co_2Cr(Al, Si)$ [5], Co-V-Ga [6,7], and Co-V-Si [8,9]. Among them, $Co_2Cr(Ga, Si)$ can occur in $L2_1$-$D0_{22}$-$L2_1$ successive transitions upon cooling from the paramagnetic (PM) state to the ferromagnetic (FM) one [4], showing an abnormal behavior of reentrant martensitic transformation (RMT). Some PM states of Co-V-Si alloys even exhibit their shape-memory effect around 700 °C [8], higher than the MT temperatures (T_M) measured in most shape-memory alloys. Compared to Ni-Mn-Ga, these off-stoichiometric Co_2YGa (Y = Cr, V) shape-memory alloys also possess relatively good mechanical properties, processability, and corrosion resistance [8,10]. They therefore have a broad prospect for applications in the areas of biomedicine, automotive, aerospace, and chemistry industries.

Similar to Ni-Mn-Ga, the MT of these Co_2-based Heusler alloys is highly alloying and composition dependent. The phenomenon of RMT was clearly observed only in some $Co_2Cr(Ga, Si)$ alloys and, there [4,11], T_M for the normal MT of $L2_1$-$D0_{22}$ and that for the RMT of $D0_{22}$-$L2_1$ were measured to change oppositely against the composition. In $Co_xCr_{79-x}Al_{10.5}Si_{10.5}$ (Cr79) alloys [5], the normal MT which results in the probably PM $D0_{22}$ martensite was found above $x = 55.8$ [12] and their T_M values increase with increasing x. Off-stoichiometric Co_2VGa alloys can have a reversible $L2_1$-$D0_{22}$ phase transition over a wide temperature range from 250 K to 500 K [6,7], whereas due to the normal MT, Co-V-Si can be as good as high-temperature shape-memory alloys above 500 K [8]. Discovering the physical mechanisms driving the alloying and composition effects on the MT and RMT is critical to design Co_2-based Heusler alloys with good shape-memory effects. However, until now, their true story was still not deeply understood.

There have been several composition-dependent quantities proposed to correlate with the composition dependence of the MT in Ni-Mn-Ga Heusler alloys, such as the number of valence electrons per atom (e/a) [13,14], the energy difference between the austenite and martensite (ΔE^{AM}) [15], the tetragonal shear modulus of the cubic $L2_1$ phase ($C' = (C_{11} - C_{12})/2$) [16,17], and the tetragonality of the martensite ($|1 - c/a|$) [18,19]. In these alloys, T_M generally increases with the increase of e/a, ΔE_{AM}, and $|1 - c/a|$ but decreases with increasing C'. The established correlation between T_M and e/a is also followed by the four groups of alloys: $Co_xCr_{78-x}Ga_{11}Si_{11}$ (Cr78) [4], Cr79 [5], $Co_xV_{50-0.5x}Ga_{50-0.5x}$ (V50) [7], and $Co_{64}V_{15}Si_{21-x}Ga_x$ (V15) [9]. However, there the relationships of $T_M \sim \Delta E^{AM}$, $T_M \sim |1 - c/a|$, and $T_M \sim C'$ have never been examined.

*Corresponding author: cmli@synu.edu.cn

Both T_M and Curie temperature (T_C) depend on the quenching temperature and the subsequent heat treatment which changes the degree of the long-range atomic order of the system [20]. Then, the site occupancy may also be a factor affecting the phase stability of these Co_2-based Heusler alloys. Dependent on the atomic occupation, the magnetism (including the magnetic excitations and the spin fluctuations) was confirmed to have a great influence on the free energy and then the elastic constants of $Co_2Cr(Ga_{1-x}Si_x)$ alloys as well in our recent paper [21]. Furthermore, the MT from $L2_1$ to tetragonal can be traced to the Jahn-Teller distortion and Fermi surface nesting [22–25]. This electronic origin as well as the effects of atomic and magnetic configurations on the MT also needs to be ascertained in each group of the Cr78, Cr79, V50, and V15 alloys.

In this paper, we will systematically investigate the composition-dependent properties and phase stability of the stoichiometric Co_2YGa as well as the off-stoichiometric Cr78 ($48 \leqslant x \leqslant 56$), Cr79 ($53 \leqslant x \leqslant 57$), V50 ($56 \leqslant x \leqslant 64$), and V15 ($4 \leqslant x \leqslant 12$) alloys with both FM and PM states, and then try to explore their physical mechanisms. The rest of the paper is arranged as follows: in Sec. II, we describe the first-principles method we used and the calculation details; in Sec. III, the equilibrium properties, crystal structures, and elastic constants of the FM and PM Co_2YGa alloys are presented, the site occupations of their off-stoichiometric alloys are determined, the composition dependence of the equilibrium properties, phase stability, and elastic constants of the four groups of FM and PM off-stoichiometric alloys are explored, their relationships of $T_M \sim \Delta E_{\mathrm{AM}}$, $T_M \sim |1 - c/a|$, and $T_M \sim C'$ are examined, and the electronic origin is discussed. Finally, we summarize the main results of this paper in Sec. IV.

II. METHODS AND CALCULATION DETAILS

Based on density-functional theory, all calculations of the present work are performed by using the first-principles exact muffin-tin-orbitals (EMTO) method [26–28]. EMTO is an improved screened Koringa-Kohn-Rostoker method. Within its theory, the one-electron Kohn-Sham equation is solved by the use of a scalar-relativistic Green's function technique and the one-electron states are determined exactly for an optimized overlapping muffin-tin potential, which is chosen as the best possible spherical approximation to the exact potential. With these improvements together with the full charge-density technique for the total energy [27,28], the EMTO method is suitable to accurately describe the total energy change with respect to anisotropic lattice distortions. Another motivation for our choice is that the coherent potential approximation (CPA) can be conveniently incorporated [29,30], which greatly facilitates the calculations of the systems with chemical disorder or magnetic disordering. In a number of former works, the accuracy of the EMTO-CPA method for the equation of state and elastic properties of metals and disordered alloys has been demonstrated [31–35].

For the present application, the Green's function is calculated for 32 complex energy points distributed exponentially on a semicircular contour. In the one-center expansion of the full charge density, the number of orbitals is truncated at eight, and the scalar-relativistic and soft-core approximations are adopted. The EMTO basis sets include s, p, d, and f components, and the exchange-correlation potential is described within the Perdew-Burke-Ernzerhof [36] generalized gradient approximation. The Brillouin zone is sampled by a uniform k-point mesh without using any smearing technique. For the stoichiometric alloys, a k-point mesh of $17 \times 17 \times 17$ is chosen whereas for the off-stoichiometric alloys, a k-point mesh of $13 \times 13 \times 13$ is adopted throughout our calculations. The Co-$3d^74s^2$, Cr-$3d^54s^1$, V-$3d^34s^2$, Ga-$4s^2p^1$, Al-$3s^2p^1$, and Si-$3s^2p^2$ are treated as valence states.

The equilibrium volume (V) and the bulk modulus (B) of both the $L2_1$ and $D0_{22}$ structures (described clearly in Ref. [3]) are determined by fitting the calculated total energies versus volume (nine data points) to a Morse function [37]. Here, the lattice parameter (c/a) of the $D0_{22}$ structure is described by the value of its equivalent face-centered tetragonal lattice so when $c/a = 1$, the $D0_{22}$ structure right means the $L2_1$ one. The stable site occupancy is obtained by comparing the free energies (F) per atom of an alloy with different site occupations at their equilibrium volume. Here, F is calculated by taking both the electronic energy (E) per atom and the chemical mixing entropy into account, expressed as

$$F = E + \frac{1}{4}k_BT\sum_{i=1}^{4}[x_i\ln x_i + (1-x_i)\ln(1-x_i)], \quad (1)$$

where x_i is the composition at each of the four sublattices, k_B is the Boltzmann constant, and $T = 300$ K.

For the cubic $L2_1$ structure, the elastic moduli C' and C_{44} are calculated by the use of volume-conserving orthorhombic and monoclinic deformations, i.e.,

$$\begin{pmatrix} 1+\epsilon_{\mathrm{o}} & 0 & 0 \\ 0 & 1-\epsilon_{\mathrm{o}} & 0 \\ 0 & 0 & \frac{1}{1-\epsilon_{\mathrm{o}}^2} \end{pmatrix} \quad (2)$$

and

$$\begin{pmatrix} 1 & \epsilon_{\mathrm{m}} & 0 \\ \epsilon_{\mathrm{m}} & 1 & 0 \\ 0 & 0 & \frac{1}{1-\epsilon_{\mathrm{m}}^2} \end{pmatrix}, \quad (3)$$

respectively. Six strains (ϵ_{o} and ϵ_{m}) from 0 to 0.05 with interval of 0.01 are used to calculate the total energies [$E(\epsilon_{\mathrm{o}})$ and $E(\epsilon_{\mathrm{m}})$]. C' and C_{44} are obtained by fitting $E(\epsilon_{\mathrm{o}})$ and $E(\epsilon_{\mathrm{m}})$ with respect to ϵ_{o} and ϵ_{m} as $E(\epsilon_{\mathrm{o}}) = E(0) + 2VC'\epsilon_{\mathrm{o}}^2$ and $E(\epsilon_{\mathrm{m}}) = E(0) + 2VC_{44}\epsilon_{\mathrm{m}}^2$, respectively. C_{11} and C_{12} are then evaluated from the bulk modulus $B = (C_{11} + 2C_{12})/3$ and the tetragonal shear elastic constant $C' = (C_{11} - C_{12})/2$. The corresponding polycrystalline elastic constants are estimated by means of the Hill average method [27].

III. RESULTS AND DISCUSSIONS

A. Crystal structure of the stoichiometric Co_2YGa alloys

Table I compares the equilibrium properties of the FM $L2_1$-Co_2YGa (Y = Sc, Ti, V, Cr, Mn, Fe, Ni, and Cu) alloys with the available experimental and theoretical results. It is found that the calculated lattice parameter (a), B, total magnetic moment (μ_{tot}), and magnetic moments on Co (μ_{Co}), Y (μ_Y), and Ga (μ_{Ga}) atoms are in good agreement with

TABLE I. Equilibrium lattice parameter (a, in Å), bulk modulus (B, in GPa), total magnetic moment (μ_{tot}, in μ_B), and magnetic moments on Co (μ_{Co}, in μ_B), Y (μ_Y, in μ_B), and Ga (μ_{Ga}, in μ_B) atoms of the FM $L2_1$-Co_2YGa (Y = Sc, Ti, V, Cr, Mn, Fe, Ni, and Cu) alloys are in comparison with those of experimental and theoretical ones from Refs. [40–47].

Y		a	B	μ_{tot}	μ_{Co}	μ_Y	μ_{Ga}
Sc		6.0788	151.3	0	0	0	0
	Exp. [40]	6.17					
	The. [38]	5.972	162.0	0			
Ti		5.8461	174.7	0.72	0.39	−0.06	−0.004
	Exp. [48–50]	5.858, 5.837		0.75			
	The. [39]	5.87	179	0.97			
V		5.7818	197.3	1.82	0.83	0.18	−0.015
	Exp. [49,51]	5.7859, 5.769		1.90			
	The. [41–43]	5.786	198	2.00	0.92	0.21	−0.008
Cr		5.7249	203.5	3.02	0.75	1.57	−0.049
	Exp. [49,52,53]	5.805, 5.741		3.01			
	The. [44,45]	5.728	208.8	3.03	0.70	1.72	−0.100
Mn		5.7223	191.4	4.10	0.68	2.82	−0.079
	Exp. [49,54,55]	5.770, 5.746					
	The. [39,44]	5.726	187		0.77	2.71	−0.056
Fe		5.7270	190.7	4.96	1.12	2.79	−0.072
	Exp. [39,49]	5.74, 5.725		5.15			
	The. [39]	5.75	187	4.99			
Ni		5.6959	181.0	2.56	1.08	0.49	−0.074
	The. [46,47]	5.68	181	2.67			
Cu		5.7142	178.5	1.20	0.60	0.05	−0.053

their previous theoretical ones [38,39,41–47]. For several of these alloys, the experimental a and μ_{tot} values are available [39,40,48–55]. In comparison, their biggest errors turn out to still be less than 1.5% and 4.5%, appearing in Co_2ScGa and Co_2VGa alloys, respectively. These results may ensure the accuracy of the EMTO calculations of the Co_2-based Heusler alloys.

With the determined equilibrium volume at the FM state, we calculate the electronic total energy change (ΔE) with respect to the tetragonal lattice distortion c/a of these stoichiometric alloys with both the FM and PM states. Shown in Fig. 1(a), in each FM alloy except for Y = Ni, ΔE of the $L2_1$ structure ($c/a = 1$) is always lower than those of the other tetragonal structures, and then the $L2_1$ structure corresponds to their ground state. For Co_2CrGa and Co_2VGa alloys, there is also another local minimum around $c/a = 1.20 - 1.25$, meaning their metastable phase at the FM state. Shown in Fig. 1(b), at the PM state, the obtained tetragonal structure in the two alloys turns out to have lower ΔE than the $L2_1$ structure. The tetragonal martensite is then stabilized instead in the PM Y = Cr and V alloys. However, in the Y = Sc, Ti, Mn, Fe, and Cu alloys with the PM ordering, ΔE still has only one minimum at $c/a = 1$. The magnetic ordering seems to have no great influence on their phase stability.

When Y = Ni, the minimum of ΔE appears around c/a = 1.40 at the FM state but near c/a = 1.35 at the PM state. It confirms that the Co_2NiGa alloy can occur in the normal MT at the two magnetic states and at the ground state; it possesses the FM tetragonal martensite. This result gives a good representation of the experimental and theoretical ones [2,47,56]. However, since the MT of Co-Ni-Ga alloys has been broadly investigated, we concentrate our investigations on the Y = Cr and V alloys below.

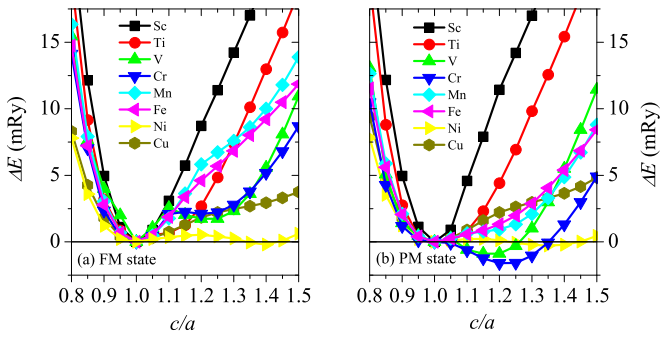

FIG. 1. Electronic total energy change (ΔE) with respect to the tetragonal lattice distortion (c/a) of Co_2YGa (Y = Sc, Ti, V, Cr, Mn, Fe, Ni, and Cu) alloys with both the FM (a) and PM (b) states. The energy of the $L2_1$ structure is taken as reference in each FM and PM alloy.

B. Site occupation and magnetic moments of the off-stoichiometric Co_2YGa alloys

In the present paper, site occupations of the off-stoichiometric Co_2YGa (Y = Cr and V) alloys are investigated and we consider three types of their compositions: Co rich ($Co_{2.1}Y_{0.9}Ga$, $Co_{2.1}YGa_{0.9}$, and $Co_{2.1}Y_{0.95}Ga_{0.95}$), Y rich ($Co_{1.9}Y_{1.1}Ga$, $Co_2Y_{1.1}Ga_{0.9}$, and $Co_{1.95}Y_{1.1}Ga_{0.95}$), and Ga rich ($Co_{1.9}YGa_{1.1}$, $Co_2Y_{0.9}Ga_{1.1}$, and $Co_{1.95}Y_{0.95}Ga_{1.1}$). For each composition, we consider two kinds of occupations: normal occupancy (the excess atom evenly occupying all the sites of the deficient atoms) and abnormal occupancy (the excess atom occupying solely the site of one of the other two atoms, and then the replaced atoms moving to the

TABLE II. Relative free energies of the FM and PM $L2_1$ austenite ($\Delta F_{\rm FM}^{L2_1}$ and $\Delta F_{\rm PM}^{L2_1}$, in mRy) and tetragonal martensite ($\Delta F_{\rm FM}^{\rm Tet}$ and $\Delta F_{\rm PM}^{\rm Tet}$, in mRy) of the off-stoichiometric Co_2YGa (Y = Cr and V) alloys at 300 K, taking the free energy of the normal site-occupation configuration as reference. Also presented in the table are their total magnetic moments in the FM $L2_1$ ($\mu_{\rm tot}^{L2_1}$, in $\mu_{\rm B}$) and tetragonal ($\mu_{\rm tot}^{\rm Tet}$, in $\mu_{\rm B}$) phases. The number to the left of the slash corresponds to Y = Cr whereas the number to the right of the slash refers to Y = V.

Type	Composition	Siteoccupancy	$\Delta F_{\rm FM}^{L2_1}$	$\Delta F_{\rm FM}^{\rm Tet}$	$\Delta F_{\rm PM}^{L2_1}$	$\Delta F_{\rm PM}^{\rm Tet}$	$\mu_{\rm tot}^{L2_1}$	$\mu_{\rm tot}^{\rm Tet}$
	Co rich							
1	$Co_{2.1}Y_{0.9}Ga$	$Co_2(Y_{0.9}Co_{0.1})Ga$	0	0	0	0	3.08/1.87	1.37/0.20
		$Co_2(Y_{0.9}Ga_{0.1})(Ga_{0.9}Co_{0.1})$	1.43/0.31	0.14/−0.51	0.16/−0.46	0.45/−0.48	2.36/1.21	1.21/0.13
2	$Co_{2.1}YGa_{0.9}$	$Co_2Y(Ga_{0.9}Co_{0.1})$	0	0	0	0	2.66/1.45	1.39/0.12
		$Co_2(Y_{0.9}Co_{0.1})(Ga_{0.9}Y_{0.1})$	−0.61/1.35	0.46/1.82	0.89/1.80	0.37/1.83	3.33/2.03	1.49/0.23
3	$Co_{2.1}Y_{0.95}Ga_{0.95}$	$Co_2(Y_{0.95}Co_{0.05})(Ga_{0.95}Co_{0.05})$	0	0	0	0	2.83/1.65	1.37/0.03
		$Co_2(Y_{0.9}Co_{0.1})(Ga_{0.95}Y_{0.05})$	−2.81/0.61	0.24/0.90	0.43/0.87	0.17/0.92	3.21/1.95	1.23/0.21
		$Co_2(Y_{0.95}Ga_{0.05})(Ga_{0.9}Co_{0.1})$	−1.88/0.18	0.05/−0.23	0.08/−0.27	0.14/−0.24	2.51/1.33	1.30/0.13
3′	$Co_{2.1}Cr_{1.1}Ga_{0.8}$	$Co_2Cr(Ga_{0.8}Co_{0.1}Cr_{0.1})$	0	0	0	0	2.94	1.14
		$Co_2(Cr_{0.9}Co_{0.1})(Ga_{0.8}Cr_{0.2})$	−0.67	0.44	0.78	2.06	3.60	1.37
		$(Co_{0.95}Cr_{0.05})_2Cr(Ga_{0.8}Co_{0.2})$	1.72	0.35	0.67	1.20	2.07	0.83
3″	$Co_{2.1}V_{0.8}Ga_{1.1}$	$Co_2(V_{0.8}Co_{0.1}Ga_{0.1})Ga$	0	0	0	0	1.61	0.16
		$Co_2(V_{0.8}Ga_{0.2})(Ga_{0.9}Co_{0.1})$	0.43	−0.67	−0.46	−0.24	1.16	0.14
		$(Co_{0.95}Ga_{0.05})_2(V_{0.8}Co_{0.2})Ga$	4.21	4.78	4.64	4.24	1.90	0.37
	***Y*rich**							
1	$Co_{1.9}Y_{1.1}Ga$	$(Co_{0.95}Y_{0.05})_2YGa$	0	0	0	0	2.73/1.37	1.51/0
		$(Co_{0.95}Ga_{0.05})_2Y(Ga_{0.9}Y_{0.1})$	2.70/2.61	3.49/3.19	2.87/2.34	2.31/2.34	3.31/1.87	1.52/0
2	$Co_2Y_{1.1}Ga_{0.9}$	$Co_2Y(Ga_{0.9}Y_{0.1})$	0	0	0	0	3.30/1.95	1.49/0
		$(Co_{0.95}Y_{0.05})_2Y(Ga_{0.9}Co_{0.1})$	1.66/2.17	0.52/0.58	0.78/1.40	1.41/1.40	2.37/0.98	1.18/0.13
3	$Co_{1.95}Y_{1.1}Ga_{0.95}$	$(Co_{0.975}Y_{0.025})_2Y(Ga_{0.95}Y_{0.05})$	0	0	0	0	3.02/1.67	1.51/0
		$(Co_{0.95}Y_{0.05})_2Y(Ga_{0.95}Co_{0.05})$	0.89/1.13	0.31/0.31	0.43/0.69	0.78/0.69	2.55/1.19	1.35/0.06
		$(Co_{0.975}Ga_{0.025})_2Y(Ga_{0.9}Y_{0.1})$	1.40/1.36	1.80/1.63	1.45/1.20	1.22/1.20	3.31/1.92	1.51/0
	Ga rich							
1	$Co_{1.9}YGa_{1.1}$	$(Co_{0.95}Ga_{0.05})_2YGa$	0	0	0	0	3.01/1.74	1.77/0
		$(Co_{0.95}Y_{0.05})_2(Y_{0.9}Ga_{0.1})Ga$	−2.18/−1.06	−3.06/−1.86	−1.84/−0.86	-1.59/-0.86	2.43/1.11	1.33/0
2	$Co_2Y_{0.9}Ga_{1.1}$	$Co_2(Y_{0.9}Ga_{0.1})Ga$	0	0	0	0	2.73/1.61	1.53/0
		$(Co_{0.95}Ga_{0.05})_2(Y_{0.9}Co_{0.1})Ga$	3.38/4.40	4.29/4.54	3.61/4.20	3.60/4.23	3.07/1.84	1.44/0.24
3	$Co_{1.95}Y_{0.95}Ga_{1.1}$	$(Co_{0.975}Ga_{0.025})_2(Y_{0.95}Ga_{0.05})Ga$	0	0	0	0	2.87/1.70	1.64/0
		$(Co_{0.95}Ga_{0.05})_2(Y_{0.95}Co_{0.05})Ga$	1.69/2.23	2.10/2.26	1.79/2.09	1.79/2.10	3.03/1.80	1.61/0.14
		$(Co_{0.975}Y_{0.025})_2(Y_{0.9}Ga_{0.1})Ga$	−1.12/−0.50	−1.58/−0.97	−0.95/−0.61	-0.80/-0.61	2.58/1.39	1.43/0
3′	$Co_{1.8}Y_{1.1}Ga_{1.1}$	$(Co_{0.9}Y_{0.05}Ga_{0.05})_2YGa$	0	0	0	0	2.72/1.39	1.55/0
		$(Co_{0.9}Y_{0.1})_2(Y_{0.9}Ga_{0.1})Ga$	−2.00/−0.80	−2.85/−2.07	−1.57/−0.75	−1.41/−0.75	2.14/0.74	1.10/0
		$(Co_{0.9}Ga_{0.1})_2Y(Ga_{0.9}Y_{0.1})$	2.58/2.76	3.29/3.02	2.71/2.22	2.27/2.22	3.31/1.77	1.59/0

sublattice of the left deficient atom). The stable site occupation is determined by comparing the free energies (ΔF) of the different site-occupation configurations relative to the normal site-occupation. The lower ΔF is, the more stable is the corresponding site configuration.

In Table II, the relative free energies of the FM and PM $L2_1$ austenite ($\Delta F_{\rm FM}^{L2_1}$ and $\Delta F_{\rm PM}^{L2_1}$) and tetragonal martensite ($\Delta F_{\rm FM}^{\rm Tet}$ and $\Delta F_{\rm PM}^{\rm Tet}$) corresponding to all the site occupations of each composition are compared. For the Co-rich Y = Cr alloys, they have the lowest $\Delta F_{\rm PM}^{L2_1}$, $\Delta F_{\rm FM}^{\rm Tet}$, and $\Delta F_{\rm PM}^{\rm Tet}$ when the excess Co atom is in the normal site, whereas when it occupies the Cr sublattice, no matter if Cr is deficient or not, these alloys possess the smallest $\Delta F_{\rm FM}^{L2_1}$. Then, in the off-stoichiometric Y = Cr alloys, the excess Co atom tends to take the Cr sublattice in the FM $L2_1$ phase whereas it is in the normal site in the other phases. However, the Co-rich Y = V alloys have the lowest $\Delta F_{\rm FM}^{L2_1}$ when the excess Co atom is in the normal site, whereas when it occupies the Ga site they possess the smallest $\Delta F_{\rm PM}^{L2_1}$, $\Delta F_{\rm FM}^{\rm Tet}$, and $\Delta F_{\rm PM}^{\rm Tet}$. In these alloys, the excess Co atom is then in the normal site in the FM $L2_1$ phase, whereas in the other phases it favors to be in the Ga site no matter if Ga is deficient or not.

When the Y atom is rich, the normal site-occupation is always energetically favorable in the off-stoichiometric alloys shown in Table II. However, similar to the off-stoichiometric Ni_2MnGa alloys where the excess Ga atom has a strong tendency to take the Mn sublattice [57], the Ga-rich Co_2YGa alloys always possess the lowest $\Delta F_{\rm FM}^{L2_1}$, $\Delta F_{\rm PM}^{L2_1}$, $\Delta F_{\rm FM}^{\rm Tet}$ as well as $\Delta F_{\rm PM}^{\rm Tet}$ when the excess Ga atom occupies the Y sublattice whereas the replaced Y atoms move to the Co site.

Also listed in Table II are the total magnetic moments corresponding to all the site occupations of each FM alloy with both the $L2_1$ ($\mu_{\rm tot}^{L2_1}$) and tetragonal ($\mu_{\rm tot}^{\rm Tet}$) structures. It is found that corresponding to the same site occupation, $\mu_{\rm tot}^{L2_1}$ is always much bigger than $\mu_{\rm tot}^{\rm Tet}$ in each composition. When Y = Cr, $\mu_{\rm tot}^{L2_1}$ is almost twice $\mu_{\rm tot}^{\rm Tet}$ whereas when Y = V, $\mu_{\rm tot}^{L2_1}$ is near ten times $\mu_{\rm tot}^{\rm Tet}$ and the latter is even less than 0.25 μ_B. This result could be attributed mainly to the magnetic moment of Co in the FM tetragonal phase ($\mu_{\rm Co}^{\rm Tet}$) being much smaller than that in the FM $L2_1$ phase ($\mu_{\rm Co}^{L2_1}$) of

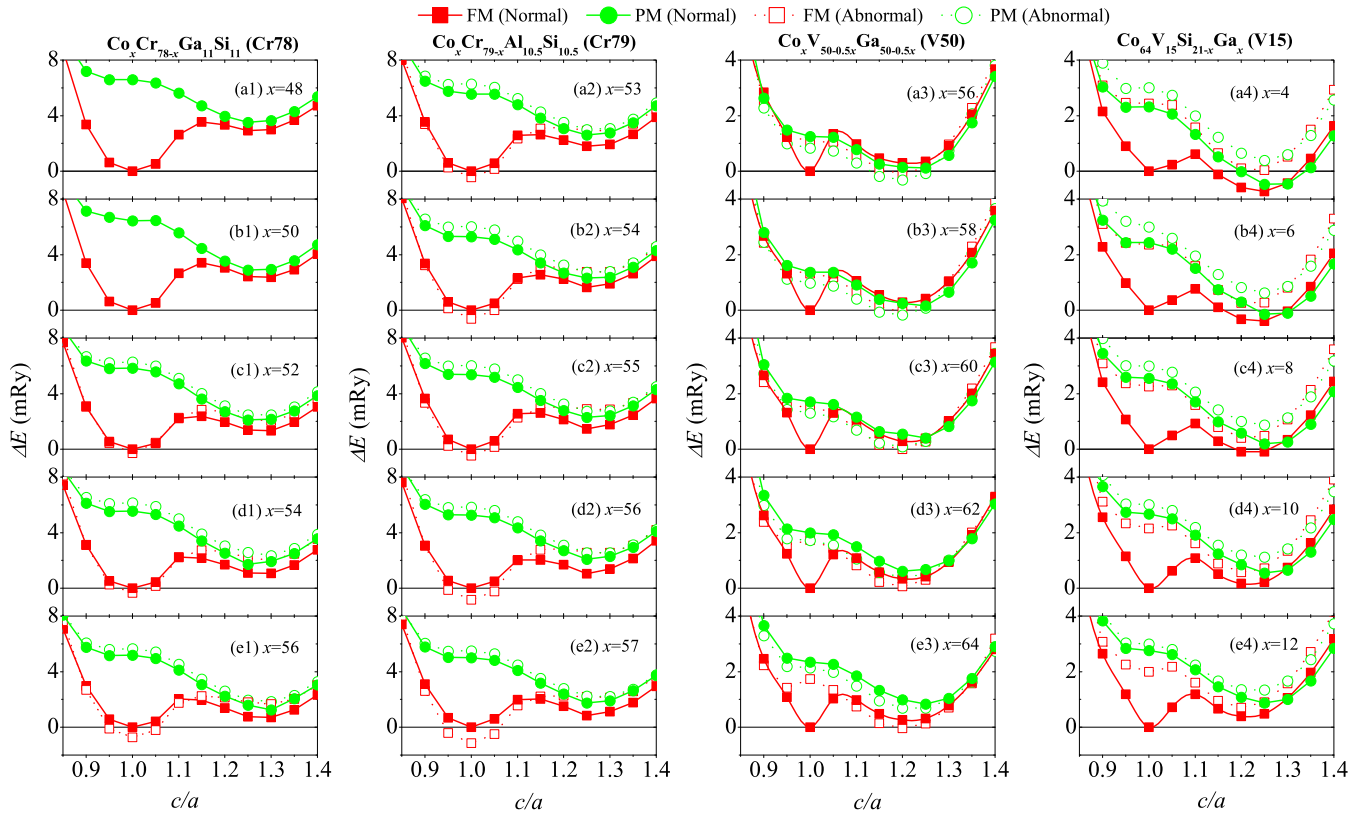

FIG. 2. Electronic total energy change (ΔE) with respect to c/a of the four groups of FM and PM off-stoichiometric alloys: Cr78 ($Co_xCr_{78-x}Ga_{11}Si_{11}$, $48 \leqslant x \leqslant 56$), Cr79 ($Co_xCr_{79-x}Al_{10.5}Si_{10.5}$, $53 \leqslant x \leqslant 57$), V50 ($Co_xV_{50-0.5x}Ga_{50-0.5x}$, $56 \leqslant x \leqslant 64$), and V15 ($Co_{64}V_{15}Si_{21-x}Ga_x$, $4 \leqslant x \leqslant 12$). Here, both results calculated with the normal and the abnormal but stable site occupations corresponding to the Co-rich alloys are presented. The energy of the FM $L2_1$ phase evaluated with the normal site occupation is a reference for each composition.

these studied $Y =$ Cr (V) alloys, where $\mu_{Co}^{L2_1}$ is around 0.62 $\sim$ 0.94 μ_B (0.42 $\sim$ 0.85 μ_B), whereas μ_{Co}^{Tet} is less than 0.15 μ_B (0.10 μ_B). In addition, in the $Y =$ Cr alloys, the magnetic moments of Cr atoms on the Ga sublattice also tend to be in the FM ordering in the cubic phase but antiferromagnetic (AFM) ordering in the tetragonal phase. Therefore, compared to the FM $L2_1$ phase, the FM tetragonal phase possesses much weaker magnetism in these off-stoichiometric Co_2YGa ($Y =$ Cr and V) alloys. This may be the reason why their stable site occupations in the FM tetragonal and the PM state of $L2_1$ and tetragonal phases are the same, whereas the site occupation of the excess Co atom in the FM $L2_1$ phase is different from that in all the other phases of the Co-rich alloys.

C. Martensitic phase transformation of the off-stoichiometric Co_2YGa alloys

1. Martensitic phase transformation

Figure 2 shows ΔE change with respect to c/a of the four groups of FM and PM alloys: Cr78 ($48 \leqslant x \leqslant 56$), Cr79 ($53 \leqslant x \leqslant 57$), V50 ($56 \leqslant x \leqslant 64$), and V15 ($4 \leqslant x \leqslant 12$). Since it has been confirmed that in the Co-rich $Y =$ Cr alloys, the excess Co atom favors to take the Cr sublattice in the FM $L2_1$ phase whereas it is in the Ga site in the other phases of the Co-rich $Y =$ V alloys, both results calculated with the abnormal and normal site occupations are presented in the figure. It is clear that in the Co-rich Cr78, Cr79, and V50 alloys, the determined site occupations in all the phases are indeed energetically favorable. In the V15 ($Co_{64}V_{15}Si_{21-x}Ga_x$) alloys, the abnormal site occupation results in both Si and Ga atoms moving to the V site, which increases more energy of the system than the excess Co atom evenly occupying the deficient V, Ga, and Si sites. The normal site occupation is therefore always energetically favorable in the V15 alloys.

For the Cr78 and Cr79 alloys shown in the first two columns of Fig. 2, respectively, at the FM state their tetragonal martensite possesses higher ΔE than the $L2_1$ austenite, and then the RMT from tetragonal to $L2_1$ tends to occur at low temperature. At the PM state, nevertheless, the relative stability between the cubic and tetragonal structures of the two groups of alloys inverses, and then the normal MT from $L2_1$ to tetragonal is realized there. These results are similar to those of the stoichiometric Co_2CrGa alloy obtained above.

Shown in the last two columns of Fig. 2, respectively, the normal MT could still be obtained in the PM V50 and V15 alloys, since there the tetragonal martensite always possesses lower energy than the $L2_1$ austenite. With the decrease of T, the magnetic excitations gradually transit the PM ordering to the FM one, preferring the relative stability of the $L2_1$ phase in all four groups of alloys. However, in the FM V50 alloys, at 0 K the evaluated ΔE of the cubic phase is still not much lower than that of the tetragonal phase, but they turn out to be almost the same. A similar result is also found in the FM state of V15 alloys with $x \geqslant 8$. For the V15 ($x = 4$ and 6) alloys, the tetragonal martensite is stabilized at the FM state as well since there it has a little lower energy than the $L2_1$ austenite.

Therefore, at finite temperature, the V50 and V15 alloys are prone to occur in the normal MT. Even when the temperature reduces to 0 K, the $L2_1$ structure just tends to coexist with the tetragonal structure in most of their compositions. Contrary to Co_2VGa alloy, the V50 and V15 alloys don't have the behavior of the RMT.

Experimentally, the normal MT has been obtained in all four groups of alloys, whereas the RMT is observed clearly in the Cr78 alloys [4]. Our investigations above have shown a good representation of these results. For the Cr79 alloys [5], nevertheless, whether they can occur in the RMT or not has not been fully found out from the experimental measurements at finite temperature. Here, we theoretically predict the possibility of their occurring in the RMT at 0 K. Besides, unlike Ni-Mn-Ga alloys where the tetragonal martensite becomes more and more stable relative to the $L2_1$ austenite with the decrease of temperature, in the studied V50 and V15 alloys the $L2_1$ phase is confirmed to get more and more stable relative to the tetragonal phase when T decreases to 0 K.

2. Correlation between the composition-dependent properties and T_M

Figure 3 shows the equilibrium volume V of the $L2_1$ phase, c/a of the tetragonal phase, $\mu_{\rm tot}^{L2_1}$, $\mu_{\rm tot}^{\rm Tet}$, $\Delta E^{\rm AM}$, and the experimental T_M values [4,5,7,9] of the four groups of off-stoichiometric alloys as a function of e/a. It is found that the present V and c/a values are very close to their experimental data [3,7,9,58]. With the increase of the composition x, e/a increases in the Cr78, Cr79, and V50 alloys whereas it decreases in the V15 alloys. However, in all four groups of alloys, V, $\mu_{\rm tot}^{L2_1}$, and $\mu_{\rm tot}^{\rm Tet}$ decrease whereas c/a, T_M, and the electronic total energy difference between the PM state of the austenite and martensite ($\Delta E_{\rm PP}^{\rm AM}$) increase monotonically with increasing e/a. The evaluated trends of $V \sim e/a$ and $c/a \sim e/a$ turn out to be the same in the FM and PM alloys. Shown in Fig. 3(e), the experimental T_M values correspond to the normal MT around or above T_C [4,5,7,9]. Compared the trend of $T_M \sim e/a$ with the established relationships of $V \sim e/a$, $c/a \sim e/a$, $\mu_{\rm tot}^{L2_1} \sim e/a$, $\mu_{\rm tot}^{\rm Tet} \sim e/a$, and $\Delta E_{\rm PP}^{\rm AM} \sim e/a$, it is confirmed that a larger c/a or $\Delta E_{\rm PP}^{\rm AM}$ but a smaller V, $\mu_{\rm tot}^{L2_1}$, or $\mu_{\rm tot}^{\rm Tet}$ corresponds to a higher T_M for the normal MT of each group of alloys.

In Fig. 3(c), the calculated electronic energy difference between the martensite and austenite ($-\Delta E_{\rm FF}^{\rm AM}$) of the FM Cr78 and Cr79 alloys is also shown with respect to e/a. With a positive value as well, $-\Delta E_{\rm FF}^{\rm AM}$ decreases with increasing e/a, contrary to the trend of $\Delta E_{\rm PP}^{\rm AM} \sim e/a$ of these alloys. It means that with the increase of e/a, the stability of the $L2_1$ phase relative to the tetragonal one gets worse and worse in the two groups of FM alloys. There, T_M corresponding to the RMT should decrease with the increase of e/a, in good agreement with the experimental result found in the Cr78 alloys [4].

Shown in Fig. 3(e), T_M for the normal MT of the Cr78 alloys are above 500 K. Correspondingly, their T_M values for the RMT are then around or below room temperature [4]. For the Cr79 alloys [5], T_M for the normal MT are just near room temperature in Fig. 3(e). Analogously, their T_M values for the RMT may then be low enough not to be easily measured. Instead, the tetragonal and $L2_1$ structures were experimentally

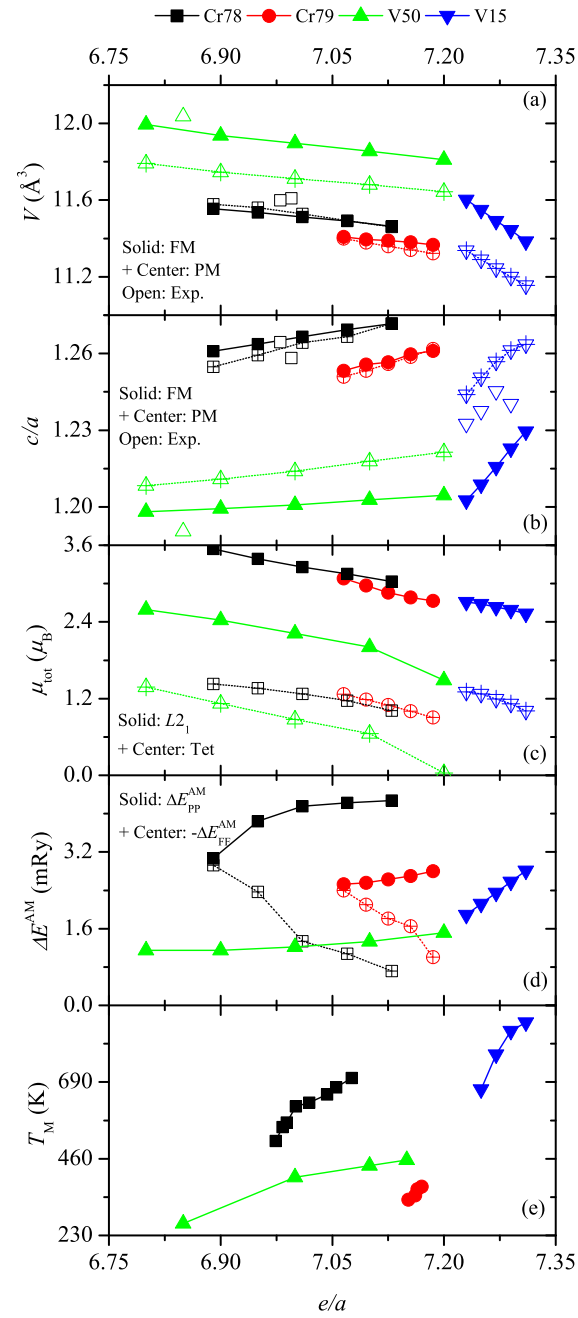

FIG. 3. Equilibrium volume (V) of the $L2_1$ phase (a), c/a of the tetragonal phase (b), $\mu_{\rm tot}^{L2_1}$ and $\mu_{\rm tot}^{\rm Tet}$ (c), the electronic total energy difference between the FM state of the martensite and austenite ($-\Delta E_{\rm FF}^{\rm AM}$) and that between the PM state of the austenite and martesnite ($\Delta E_{\rm PP}^{\rm AM}$) (d), and the experimental T_M values (e) of the Cr78 ($48 \leqslant x \leqslant 56$), Cr79 ($53 \leqslant x \leqslant 57$), V50 ($56 \leqslant x \leqslant 64$), and V15 ($4 \leqslant x \leqslant 12$) alloys as a function of e/a. The cited experimental V and c/a data are from Refs. [3,7,9,58], and the experimental T_M values are from Refs. [4,5,7,9].

observed coexisting there at low temperature [5]. Although a larger $\mu_{\rm tot}^{L2_1}$ or $\mu_{\rm tot}^{\rm Tet}$ corresponds to a lower T_M for the normal MT in Fig. 3, the high magnetization (i.e., high $\mu_{\rm tot}^{L2_1}$ or $\mu_{\rm tot}^{\rm Tet}$ value) of a FM alloy may ensure its T_M value for the RMT to be high enough near the room temperature. Shown in Fig. 3, a higher $\mu_{\rm tot}^{L2_1}$ or $\mu_{\rm tot}^{\rm Tet}$ indeed means a bigger $-\Delta E_{\rm FF}^{\rm AM}$ in the

TABLE III. Static elastic constants C_{11}, C_{12}, and C_{44}, tetragonal shear elastic constant [$C' = (C_{11} - C_{12})/2$], shear modulus (G), Young modulus (E), Debye temperature (Θ, in K), elastic anisotropy [$A = 2C_{44}/(C_{11} - C_{12})$], and G/B of $L2_1$-Co_2YGa (Y = Sc, Ti, V, Cr, Mn, Fe, Ni, and Cu) alloys with both the FM and PM (shown in the parentheses) states. All the elastic constants are in the unit of GPa. The cited theoretical data are from Refs. [38,46,59].

Y		C_{11}	C_{12}	C_{44}	C'	G	E	Θ	A	G/B
Sc		250.3(249.5)	101.8(102.2)	103.1(103.0)	74.2(73.7)	90.4(90.1)	226.1(225.5)	492.7(491.9)	1.39(1.40)	0.51(0.50)
	The. [38]	266.7	109.7	98.0	78.5	89.7	227.2		1.25	0.55
Ti		203.8(201.0)	160.1(172.6)	116.0(117.9)	21.8(14.2)	57.8(47.9)	156.0(132.2)	392.0(358.0)	5.31(8.31)	0.33(0.26)
V		277.7(193.4)	157.1(179.1)	143.1(113.8)	58.3(7.1)	100.8(34.1)	258.4(96.2)	507.1(299.6)	2.46(15.95)	0.51(0.19)
	The. [59]	266.5	162.1	126.8	52.2	88.5			2.43	0.45
Cr		240.3(180.6)	185.1(176.2)	137.3(123.5)	27.6(2.2)	70.4(20.0)	189.3(57.8)	424.2(229.5)	4.97(56.39)	0.35(0.11)
	The. [59]	233.0	182.8	136.8	25.1	67.3			5.45	0.34
Mn		235.7(235.3)	169.2(196.9)	141.6(136.4)	43.2(19.2)	77.7(59.6)	205.4(163.6)	441.6(389.2)	3.27(7.10)	0.41(0.28)
	The. [59]	254.9	165.3	142.7	44.8	88.8			3.19	0.45
Fe		232.8(216.5)	169.7(179.9)	127.5(125.0)	31.5(18.3)	71.6(55.6)	190.9(152.2)	423.8(375.0)	4.04(6.82)	0.38(0.29)
Ni		195.4(191.7)	173.8(172.5)	137.7(140.1)	10.8(9.6)	45.9(43.7)	126.9(121.3)	338.6(330.6)	12.73(14.60)	0.25(0.24)
	The. [46]	197	187	120	5					
Cu		202.8(193.4)	166.4(162.2)	133.5(133.4)	18.2(15.6)	57.5(53.5)	155.7(145.5)	374.5(361.6)	7.33(8.55)	0.32(0.31)

Cr78 and Cr79 alloys. Thus, the high magnetization prefers the relative stability of their cubic $L2_1$ phase at both the FM and PM states.

Besides, the relatively big difference of the magnetization between the austenite and martensite may also favor the occurrence of the RMT. Compared to the FM Cr78 and Cr79 alloys in Fig. 3(c), the difference between $\mu_{\rm tot}^{L2_1}$ and $\mu_{\rm tot}^{\rm Tet}$ is much smaller in the FM V50 and V15 alloys, where the $L2_1$ phase is then not much lower than the tetragonal phase in energy. However, shown in Table II, the Y = Cr and V alloys are close to their stoichiometric compositions. With the same composition, although the $\mu_{\rm tot}^{L2_1}$ and $\mu_{\rm tot}^{\rm Tet}$ values of the Y = V alloy are much smaller than those corresponding to the Y = Cr alloy, the difference between $\mu_{\rm tot}^{L2_1}$ and $\mu_{\rm tot}^{\rm Tet}$ of the former is generally not much smaller than that of the latter. Similar to Co_2CrGa and Co_2VGa alloys, all the off-stoichiometric Y = Cr and V alloys shown in the table turn out to have the behavior of the RMT and at 0 K, they possess the $L2_1$ structure.

D. Elastic property

1. *Elastic constants of the stoichiometric* Co_2YGa *alloys*

Table III lists the Y dependence of 0 K C_{11}, C_{12}, C_{44}, C', shear modulus (G), Young modulus (E), Debye temperature (Θ), elastic anisotropy [$A = 2C_{44}/(C_{11} - C_{12})$], and G/B of the FM and PM (shown in the parentheses) $L2_1$-Co_2YGa alloys. It is shown that the present elastic constants of the Y = Sc, V, Cr, Mn, and Ni alloys are in line with their first-principles results from the projected augmented-wave calculations [38,46,59]. Since the ground state of Co_2ScGa alloy is close to the PM state, calculated with the FM and PM orderings its elastic constants are almost the same. For the other compositions, nevertheless, their evaluated C_{11} as well as C', G, E, and Θ at the PM state are always smaller than those at the FM state, whereas A of the PM alloy is larger than that of the FM alloy. The PM ordering tends to soften the elastic constants of these alloys. Especially for Co_2CrGa (or Co_2VGa), the C', G, E, and Θ values at the PM state are merely their respective values at the FM state 7.93% (12.23%), 28.4% (33.8%), 30.5% (37.2%), and 54.1% (59.1%), whereas the A value at the PM state is about 11.3 (6.48) times its correspondent at the FM state.

At the FM state, only Co_2NiGa alloy can occur in the MT from $L2_1$ to tetragonal. Correspondingly, its C', G, E, and Θ values are the smallest, whereas the A value is the biggest among all the FM alloys in Table III. At the PM state, these elastic constants of the Co_2NiGa alloy change relatively small, and the relative stability between its austenite and martensite is then similar at the two magnetic states, as shown in Fig. 1. However, in the PM Y = Cr and V alloys, their C', G, E, and Θ get smaller whereas A is bigger than those of Co_2NiGa. As a result, the normal MT is obtained in the two PM alloys as well in Fig. 1(b). For the other PM alloys, their C', G, E, and Θ are still larger whereas A is smaller than those of Co_2NiGa alloy. Then, these alloys still possess the cubic $L2_1$ structure at the PM state.

The plastic property of a material has been related to the ratio of the shear and bulk modulus (G/B). A high value of G/B (greater than ~0.57) generally means the inherent crystalline brittleness (ICB) of a bulk material. From Table III, we find that the G/B values of these alloys are all below this critical value and hence their ICB is low. In comparison with the FM ordering, the PM ordering also decreases the G/B of these stoichiometric alloys, especially for Co_2CrGa and Co_2VGa alloys.

2. *Elastic constants of the off-stoichiometric* Co_2YGa *alloys*

Table IV lists the static elastic constants C_{11}, C_{12}, and C_{44} of the four groups of off-stoichiometric $L2_1$-Co_2YGa alloys with respect to the composition x as well as e/a. In each group of alloys, C_{11}, C_{12}, and C_{44} all change monotonically with respect to x (or e/a). In the Cr78 and V50 alloys, C_{11} and C_{12} decrease but C_{44} increases with increasing e/a at the FM state whereas, at the PM state, all of them tend to increase with e/a. In the two magnetic states of Cr79 alloys, C_{12} increases but C_{44} decreases with increasing e/a whereas in the V15 alloys with both the magnetic states, C_{12} decreases but C_{11} and C_{44} increase with e/a. For C_{11} of the Cr79 alloys, it increases at

TABLE IV. x (and e/a) dependence of the static elastic constants C_{11}, C_{12}, and C_{44} of the $L2_1$ phase of Cr78 ($48 \leqslant x \leqslant 56$), Cr79 ($53 \leqslant x \leqslant 57$), V50 ($56 \leqslant x \leqslant 64$), and V15 ($4 \leqslant x \leqslant 12$) alloys with both the FM and PM (shown in the parentheses) states.

Alloys	x	e/a	C_{11} (GPa)	C_{12} (GPa)	C_{44} (GPa)
Cr78	48	6.89	249.9(181.4)	164.1(189.5)	146.6(127.8)
	50	6.95	247.7(181.8)	164.1(192.6)	148.7(128.4)
	52	7.01	243.8(182.4)	164.1(195.1)	150.8(129.1)
	54	7.07	241.1(182.5)	163.9(195.7)	152.0(129.5)
	56	7.13	240.0(182.6)	163.8(196.9)	153.5(130.0)
Cr79	53	7.065	241.6(181.9)	142.6(191.8)	152.8(130.6)
	54	7.095	241.8(181.7)	144.1(191.8)	150.7(130.3)
	55	7.125	241.9(181.6)	145.6(191.8)	149.4(130.1)
	56	7.155	242.1(181.4)	147.0(191.8)	148.8(129.9)
	57	7.185	242.2(181.3)	147.6(191.9)	148.4(129.7)
V50	56	6.8	207.0(200.8)	141.1(191.8)	126.5(114.9)
	58	6.9	197.0(204.9)	131.5(196.1)	129.8(118.1)
	60	7.0	191.2(206.9)	126.5(199.8)	133.5(121.2)
	62	7.1	182.9(207.2)	122.4(202.3)	134.0(123.5)
	64	7.2	172.3(207.5)	117.7(204.0)	134.4(125.0)
V15	4	7.31	219.3(201.6)	169.2(211.2)	130.2(120.6)
	6	7.29	220.7(202.1)	166.9(209.1)	131.5(121.0)
	8	7.27	222.1(202.5)	165.3(206.7)	132.7(121.5)
	10	7.25	223.4(203.2)	163.4(204.7)	133.5(121.7)
	12	7.23	224.2(203.9)	162.6(202.6)	134.3(121.8)

the FM state but decreases at the PM state with the increase of e/a. In all these FM alloys, C_{11} is always much larger than C_{12}, whereas in the PM Cr78, Cr79, and V15 ($x \leqslant 10$) alloys, C_{11} is smaller than C_{12}, giving their negative C' values. In these alloys, the PM $L2_1$ phase is then mechanically unstable as well at 0 K.

Figure 4 shows the e/a dependence of C', G, E, Θ, A, and G/B of the four groups of FM $L2_1$ alloys. In the Cr78 and Cr79 alloys, the FM $L2_1$ phase corresponds to the ground state. Their C', G, E, and Θ of the phase are also much bigger than those of the FM V50 and V15 alloys where, nevertheless, the normal MT from $L2_1$ to tetragonal is then prone to occur at finite temperature. With increasing e/a, all the C', G, E, and Θ values decrease whereas A increases in each group of alloys. The decrease of C' but the increase of A with e/a disfavors the stability of the FM $L2_1$ phase, which further suppresses the occurrence of the RMT but promotes the behavior of the normal MT. Correspondingly, the T_M values for the RMT of the Cr78 and Cr79 alloys decrease whereas those for the MT of the V50 and V15 alloys increase with increasing e/a. Among the four groups of alloys, the V15 alloys possess the biggest e/a ratio, and then they have the smallest C' [Fig. 4(a)] but the biggest A [Fig. 4(e)] values. Consequently, they also possess the highest experimental T_M values in Fig. 3(e).

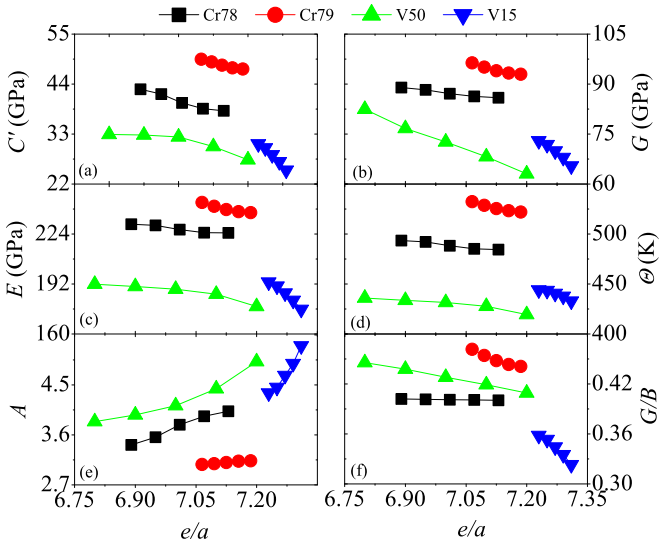

FIG. 4. e/a dependence of the static tetragonal shear elastic constant ($C' = (C_{11} - C_{12})/2$) (a), shear modulus (G) (b), Young modulus (E) (c), Debye temperature (Θ) (d), elastic anisotropy [$A = 2C_{44}/(C_{11} - C_{12})$] (e), and G/B (f) of the FM $L2_1$ phase of Cr78 ($48 \leqslant x \leqslant 56$), Cr79 ($53 \leqslant x \leqslant 57$), V50 ($56 \leqslant x \leqslant 64$), and V15 ($4 \leqslant x \leqslant 12$) alloys.

Shown in Fig. 4(f), G/B ratio decreases with increasing e/a in each group of alloys except for Cr78, where it is almost composition independent. It indicates that the ICB of all these Cr79, V50, and V15 alloys get lower and lower with the increase of e/a. Then, with the biggest e/a ratio, the V15 alloys also possess the smallest G/B among the four groups of alloys in the figure. They were therefore experimentally found showing better mechanical properties than Ni-Mn-Ga alloys [8,9].

E. Electronic structure

Similar to Ni-Mn-Ga [22–25], the MT of Co_2CrGa alloy has been also demonstrated to be closely related to the minority (spin-down) density of states (DOS) around Fermi level of the cubic $L2_1$ phase in our previous work [21]. The more electrons are distributed around the Fermi level in the minority DOS, the more unstable the system, due to the

TABLE V. Total density of states at the Fermi level of the FM $[N(E_F)^{\uparrow}_{\rm FM}$ and $N(E_F)^{\downarrow}_{\rm FM}$ for the spin-up and spin-down parts, respectively, in states/Ry] and PM $[N(E_F)_{\rm PM}$, in states/Ry] $L2_1$-Co_2YGa (Y = Sc, Ti, V, Cr, Mn, Fe, Ni, and Cu) alloys, together with the spin polarization (P) of these FM cubic alloys.

Y	$N(E_F)^{\uparrow}_{\rm FM}$	$N(E_F)^{\downarrow}_{\rm FM}$	$N(E_F)_{\rm PM}$	P
Sc	1.810	1.810	1.810	0
Ti	7.241	4.977	7.514	18.5
V	14.153	0.006	11.367	99.9
Cr	17.999	0.038	13.884	99.6
Mn	8.090	1.667	7.967	65.8
Fe	4.366	1.830	7.962	40.9
Ni	3.888	11.350	13.123	49.0
Cu	16.848	2.328	9.428	75.7

Jahn-Teller effect [22,23]. Here, to understand the atomistic origin of the phase stability of $L2_1$-Co_2YGa alloys, we compare their total DOS at the Fermi level corresponding to the FM $[N(E_F)^{\uparrow}_{\rm FM}$ and $N(E_F)^{\downarrow}_{\rm FM}$, meaning the spin-up and spin-down parts, respectively] and PM ($N(E_F)_{\rm PM}$) states, as shown in Table V. At the FM state, Co_2NiGa alloy has the biggest $N(E_F)^{\downarrow}_{\rm FM}$ and, correspondingly, it can occur in the MT and possesses the tetragonal structure at the ground state. At the PM state, $N(E_F)_{\rm PM}$ gets much bigger than $N(E_F)^{\downarrow}_{\rm FM}$ in all the alloys except for Co_2ScGa. The redistribution of electrons increases the energy of the system and then enhances the Jahn-Teller instability of the PM $L2_1$ phase. In these PM alloys without Y = Sc, C' is thus smaller whereas A is bigger than their correspondents at the FM state. For Co_2CrGa and Co_2VGa alloys, their $N(E_F)_{\rm PM}$ values are even larger than $N(E_F)^{\downarrow}_{\rm FM}$ of Co_2NiGa alloy, and then at the PM state they can occur in the normal MT as well as Co_2NiGa alloy. However, for the other PM Co_2YGa alloys, their $N(E_F)_{\rm PM}$ values are still smaller than $N(E_F)^{\downarrow}_{\rm FM}$ of Co_2NiGa alloy, and correspondingly they are stabilized by the cubic $L2_1$ structure at the two magnetic states. From the calculated spin polarization ($P = |N(E_F)^{\uparrow}_{\rm FM} - N(E_F)^{\downarrow}_{\rm FM}|/|N(E_F)^{\uparrow}_{\rm FM} + N(E_F)^{\downarrow}_{\rm FM}| \times 100\%$) shown in the table, it is also confirmed that in the FM $L2_1$ ground phase, both Co_2CrGa and Co_2VGa alloys exhibit a nearly half-metallic behavior, which is in good agreement with the previous theoretical results [43,53].

Figure 5 compares the total DOS of the FM and PM $L2_1$ and tetragonal phases of the Cr78 (x = 48 and 56), Cr79 (x = 53 and 57), V50 (x = 56 and 64), and V15 (x = 4 and 12) alloys. In the FM $L2_1$ phase, there is always a pseudogap around the Fermi level in the minority DOS of these alloys, i.e., their $N(E_F)^{\downarrow}_{\rm FM}$ values are much bigger than 0. This result indicates that all four groups of off-stoichiometric alloys possess the non-half-metallic property in the FM $L2_1$ phase. For the Cr78 and Cr79 alloys, upon tetragonal distortion, the pseudogap gets shallower and narrower, which increases the states near the Fermi level and then enhances the energy of the system. The FM $L2_1$ phase thus corresponds to their ground state. At the PM state, a big peak appears right at the Fermi level instead of in the cubic phase. Upon tetragonal distortion, it splits and there a pseudogap is formed. The tetragonal structure is thus more stable than the $L2_1$ structure

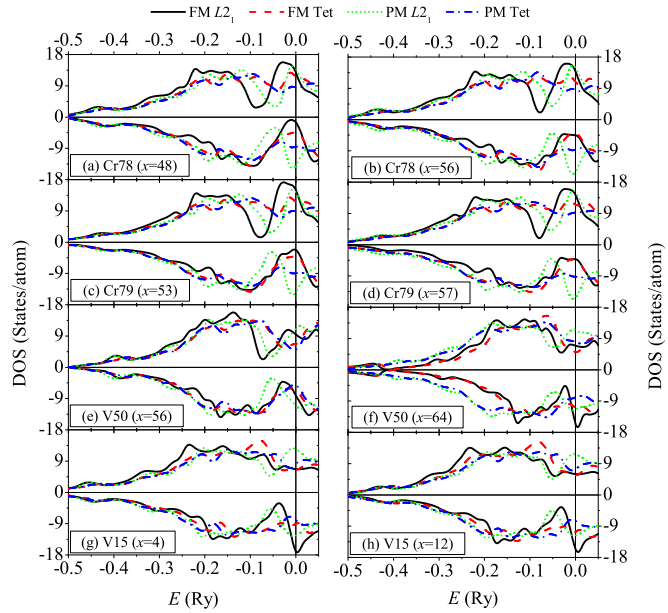

FIG. 5. Total density of states (DOS) of the FM and PM $L2_1$ and tetragonal Cr78 (x = 48 (a) and 56 (b)), Cr79 [x = 53 (c) and 57 (d)], V50 [x = 56 (e) and 64 (f)], and V15 [x = 4 (g) and 12 (h)] alloys. The vertical lines indicate the Fermi level.

in the two groups of PM alloys. With increasing x (or e/a), the pseudogap in the FM $L2_1$ phase becomes shallower and the peak in the PM $L2_1$ phase gets a little bigger, whereas there is almost no great change found in the DOS of the two magnetic states of the tetragonal phase. As a result, with the increase of e/a, the relative stability of the cubic $L2_1$ phase gets worse and worse at both the FM and PM states. It favors T_M for the RMT decreasing but that for the normal MT increasing with e/a.

In both the FM and PM $L2_1$ phases of V50 and V15 alloys, the pseudogap in the minority DOS is below the Fermi level. It results that the antibonding states (right side of the pseudogap) are occupied as well as the bonding states (left side of the pseudogap), which disfavors the stability of the cubic structure. Upon tetragonal distortion, the pseudogap shifts toward a higher energy level, resulting that its valley is right at the Fermi level in the two magnetic states of the tetragonal phase. It means there the bonding states are fully occupied whereas the antibonding states are empty, preferring the stability of the system. Therefore, they are prone to occur in the normal MT at both the FM and PM states. With increasing e/a, more and more antibonding states are occupied around the Fermi level in the minority DOS of the FM $L2_1$ phase, whereas there is almost no great change found in the DOS of the other phases. It favors the MT from $L2_1$ to tetragonal in the V50 and V15 alloys, and then their experimental T_M values increase with e/a.

IV. SUMMARY

Using the first-principles EMTO-CPA method, we have systematically investigated the composition-dependent crystal structure, magnetic moments, phase stability, and elastic properties of the stoichiometric Co_2YGa as well as the

off-stoichiometric Cr78, Cr79, V50, and V15 alloys with both the FM and PM states. The main results are summarized as follows:

(1) At both the FM and PM states, the stoichiometric Co_2YGa (Y = Sc, Ti, Mn, Fe, and Cu) alloys possess the cubic $L2_1$ structure, whereas the Co_2NiGa alloy has the tetragonal structure. Co_2CrGa and Co_2VGa alloys have the $L2_1$ structure at the FM state but the tetragonal structure at the PM state.

(2) In the off-stoichiometric Co_2YGa (Y = Cr and V) alloys, the excess Y atom is always in the normal site, whereas the excess Ga atom has strong tendency to take the Y sublattice; the excess Co atom tends to take the Y sublattice in the FM $L2_1$ phase but the normal site in the other phases when Y = Cr, whereas when Y = V it is in the normal site in the FM $L2_1$ phase but the Ga sublattice in the other phases. The determined site occupations are also followed by the off-stoichiometric Cr78, Cr79, and V50 alloys. In the V15 alloys, nevertheless, the normal site occupation is always energetically favorable.

(3) The Cr78 and Cr79 alloys can occur in the normal MT at the PM state but the RMT at the FM state. Nevertheless, only the normal MT is obtained in the V50 and V15 alloys, where the small difference of the magnetization between the austenite and martensite is supposed to suppress the RMT. In the four groups of alloys, a larger c/a or ΔE_{PP}^{AM} but a smaller V, $\mu_{tot}^{L2_1}$, or μ_{tot}^{Tet} corresponds to a higher T_M for the normal MT. In the Cr78 and Cr79 alloys, the T_M values for the RMT are also predicted to decrease with increasing e/a.

(4) The PM ordering tends to soften the elastic constants of all these $L2_1$ alloys. For the PM $L2_1$-Co_2CrGa and Co_2VGa alloys, their C', G, E, and Θ values get smaller whereas A is bigger than those corresponding to Co_2NiGa, and then they can occur in the MT as well. For the PM $L2_1$ phase of Cr78, Cr79, and V15 ($x \leqslant 10$) alloys, their static C' values even turn out to be negative, and then they are mechanically unstable as well at 0 K. In the four groups of FM $L2_1$ alloys, C', G, E, Θ, and G/B decrease whereas A increases with increasing e/a, which favors T_M for their RMT decreasing but that for their normal MT increasing with e/a.

(5) Among all the stoichiometric alloys with the FM $L2_1$ phase, Co_2NiGa alloy has the biggest $N(E_F)_{FM}^{\downarrow}$ and, correspondingly it can occur in the MT. For $L2_1$-Co_2CrGa and Co_2VGa alloys, their $N(E_F)_{PM}$ values are even larger than $N(E_F)_{FM}^{\downarrow}$ of $L2_1$-Co_2NiGa alloy. They thus can occur in the normal MT at the PM state as well. The composition dependence of the MT of the four groups of off-stoichiometric alloys could be also explained from their minority DOS around the Fermi level of the $L2_1$ parent phase by means of the Jahn-Teller effect.

ACKNOWLEDGMENTS

The authors acknowledge financial support from the NSFC under Grants No. 11674233 and No. 51301176, the China postdoctoral Science Foundation under Grants No. 2013M530133 and No. 2014T70264, and Natural Science Foundation of Liaoning Province under Grants No. 2019-MS-287, No. 2019-ZD-0484, and No. L201602672. The MoST of China under Grant No. 2014CB644001 is also acknowledged for financial support.

[1] S. Fujii, S. Ishida, and S. Asano, J. Phys. Soc. Jpn. **58**, 3657 (1989).
[2] M. Wuttig, J. Li, and C. Craciunescu, Scr. Mater. **44**, 2393 (2001).
[3] X. Xu, T. Omori, M. Nagasako, A. Okubo, R. Y. Umetsu, T. Kanomata, K. Ishida, and R. Kainuma, Appl. Phys. Lett. **103**, 164104 (2013).
[4] X. Xu, M. Nagasako, M. Kataoka, R. Y. Umetsu, T. Omori, T. Kanomata, and R. Kainuma, Phys. Rev. B **91**, 104434 (2015).
[5] T. Odaira, X. Xu, A. Miyake, T. Omori, M. Tokunaga, and R. Kainuma, Scr. Mater. **153**, 35 (2018).
[6] C. Q. Liu, Z. Li, Y. L. Zhang, Y. S. Huang, M. F. Ye, X. D. Sun, G. J. Zhang, Y. M. Cao, K. Xu, and C. Jing, Appl. Phys. Lett. **112**, 211903 (2018).
[7] X. Xu, A. Nagashima, M. Nagasako, T. Omori, T. Kanomata, and R. Kainuma, Appl. Phys. Lett. **110**, 121906 (2017).
[8] H. X. Jiang, X. Xu, T. Omori, M. Nagasako, J. J. Ruan, S. Y. Yang, C. P. Wang, X. J. Liu, and R. Kainuma, Mater. Sci. Eng. A **676**, 191 (2016).
[9] H. X. Jiang, C. P. Wang, W. W. Xu, X. Xu, S. Y. Yang, R. Kainuma, and X. J. Liu, Mater. Des. **116**, 300 (2017).
[10] S. Sahay and B. Goswami, Solid State Phenom. **150**, 197 (2009).
[11] X. Xu, T. Omori, M. Nagasako, T. Kanomata, and R. Kainuma, Appl. Phys. Lett. **107**, 181904 (2015).
[12] K. Hirata, X. Xu, T. Omori, M. Nagasako, and R. Kainuma, J. Alloys Compd. **642**, 200 (2015).
[13] Y. Xin, Y. Li, C. B. Jiang, and H. B. Xu, Mater. Sci. Forum **475–479**, 1991 (2005).
[14] C. Seguí, J. Pons, and E. Cesari, Acta Mater. **55**, 1649 (2007).
[15] J. Chen, Y. Li, J. X. Shang, and H. B. Xu, Appl. Phys. Lett. **89**, 231921 (2006).
[16] C. Bungaro, K. M. Rabe, and A. Dal Corso, Phys. Rev. B **68**, 134104 (2003).
[17] M. Stipcich, L. Mañosa, A. Planes, M. Morin, J. Zarestky, T. Lograsso, and C. Stassis, Phys. Rev. B **70**, 054115 (2004).
[18] S. Banik, R. Ranjan, A. Chakrabarti, S. Bhardwaj, N. P. Lalla, A. M. Awasthi, V. Sathe, D. M. Phase, P. K. Mukhopadhyay, D. Pandey, and S. R. Barman, Phys. Rev. B **75**, 104107 (2007).
[19] N. Lanska, O. Söderberg, A. Sozinov, Y. Ge, K. Ullakko, and V. K. Lindroos, J. Appl. Phys. **95**, 8074 (2004).
[20] V. Sánchez-Alarcos, V. Recarte, J. I. Pérez-Landazábal, and G. J. Cuello, Acta Mater. **55**, 3883 (2007).
[21] C. M. Li, Y. F. Hu, W. J. Feng, and R. Z. Huang, Phys. Rev. B **98**, 224107 (2018).
[22] A. Ayuela, J. Enkovaara, K. Ullakko, and R. M. Nieminen, J. Phys.: Condens. Matter **11**, 2017 (1999).
[23] A. Ayuela, J. Enkovaara, and R. M. Nieminen, J. Phys.: Condens. Matter **14**, 5325 (2002).
[24] C. P. Opeil, B. Mihaila, R. K. Schulze, L. Mañosa, A. Planes, W. L. Hults, R. A. Fisher, P. S. Riseborough, P. B. Littlewood, J. L. Smith, and J. C. Lashley, Phys. Rev. Lett. **100**, 165703 (2008).

[25] V. V. Godlevsky and K. M. Rabe, Phys. Rev. B **63**, 134407 (2001).
[26] O. K. Andersen, O. Jepsen, and G. Krier, in *Lectures on Methods of Electronic Sutructure Calculations*, edited by V. Kumar, O. K. Andersen, and A. Mookerjee (World Scientific, Singapore, 1994), pp. 63–124.
[27] L. Vitos, *Computational Quantum Mechanics for Materials Engineers* (Springer-Verlag, London, 2007).
[28] L. Vitos, Phys. Rev. B **64**, 014107 (2001).
[29] L. Vitos, I. A. Abrikosov, and B. Johansson, Phys. Rev. Lett. **87**, 156401 (2001).
[30] B. L. Györffy, Phys. Rev. B **5**, 2382 (1972).
[31] L. Vitos, P. A. Korzhavyi, and B. Johansson, Nat. Mater. **2**, 25 (2003).
[32] Z. H. Dong, W. Li, S. Schönecker, S. Lu, D. F. Chen, and L. Vitos, Phys. Rev. B **92**, 224420 (2015).
[33] D. Y. Kim, J. Hong, and L. Vitos, Phys. Rev. B **90**, 144413 (2014).
[34] C. M. Li, Q. M. Hu, R. Yang, B. Johansson, and L. Vitos, Phys. Rev. B **91**, 174112 (2015).
[35] C. M. Li, R. Yang, B. Johansson, and L. Vitos, Phys. Rev. B **94**, 214108 (2016).
[36] J. P. Perdew, K. Burke, and M. Ernzerhof, Phys. Rev. Lett. **77**, 3865 (1996).
[37] V. L. Moruzzi, J. F. Janak, and K. Schwarz, Phys. Rev. B **37**, 790 (1988).
[38] Y. Li, H. K. Yuan, J. H. Xia, G. L. Zhang, M. M. Zhong, A. L. Kuang, G. Z. Wang, X. R. Zheng, and H. Chen, Eur. Phys. J. Appl. Phys. **70**, 31001 (2015).
[39] J. N. Gonçalves, N. M. Fortunato, J. S. Amaral, and V. S. Amaral, J. Magn. Magn. Mater. **428**, 362 (2017).
[40] A. W. Carbonari, R. N. Saxena, W. Pendl, Jr., J. Mestnik Filho, R. N. Attili, M. Olzon-Dionysio, and S. D. de Souza, J. Magn. Magn. Mater. **163**, 313 (1996).
[41] T. Kanomata, Y. Chieda, K. Endo, H. Okada, M. Nagasako, K. Kobayashi, R. Kainuma, R. Y. Umetsu, H. Takahashi, Y. Furutani, H. Nishihara, K. Abe, Y. Miura, and M. Shirai, Phys. Rev. B **82**, 144415 (2010).
[42] P. J. Webster and K. R. A. Ziebeck, J. Phys. Chem. Solid. **34**, 1647 (1973).
[43] A. Bentouaf, R. Mebsout, and B. Aïssa, J. Alloys Compd. **771**, 1062 (2019).
[44] B. Hamad, J. Appl. Phys. **115**, 113905 (2014).
[45] S. Ram, M. R. Chauhan, K. Agarwal, and V. Kanchana, Philos. Mag. Lett. **91**, 545 (2011).
[46] R. Arróyave, A. Junkaew, A. Chivukula, S. Bajaj, C.-Y. Yao, and A. Garay, Acta Mater. **58**, 5220 (2010).
[47] M. Siewert, M. E. Gruner, A. Dannenberg, A. Hucht, S. M. Shapiro, G. Xu, D. L. Schlagel, T. A. Lograsso, and P. Entel, Phys. Rev. B **82**, 064420 (2010).
[48] A. Okubo, R. Y. Umetsu, M. Nagasako, A. Fujita, R. Kainuma, and K. Ishida, Scr. Mater. **59**, 830 (2008).
[49] R. Y. Umetsu, K. Kobayashi, R. Kainuma, Y. Yamaguchi, K. Ohoyama, A. Sakuma, and K. Ishida, J. Alloys Compd. **499**, 1 (2010).
[50] K. R. A. Ziebeck and P. J. Webster, J. Phys. Chem. Solids. **35**, 1 (1974).
[51] K. Schroeder, J. Waybright, P. Kharel, W. Zhang, S. Valloppilly, J. Herran, P. Lukashev, Y. Huh, R. Skomski, and D. J. Sellmyer, AIP Adv. **8**, 056431 (2018).
[52] K. H. J. Buschow, P. G. van Engen, and R. Jongebreur, J. Magn. Magn. Mater. **38**, 1 (1983).
[53] R. Y. Umetsu, K. Kobayashi, R. Kainuma, A. Fujita, and K. Fukamichi, Appl. Phys. Lett. **85**, 2011 (2004).
[54] P. J. Brown, K. U. Neumann, P. J. Webster, and K. R. A. Ziebec, J. Phys.: Condens. Matter **12**, 1827 (2000).
[55] P. J. Webster and K. R. A. Ziebeck, *Magnetic Properties of Metals, Landolt-Börnstein*, New Series III/19c (Springer, Berlin, 1988), p. 88.
[56] A. Talapatra, R. Arróyave, P. Entel, I. Valencia-Jaime, and A. H. Romero, Phys. Rev. B **92**, 054107 (2015).
[57] Q. M. Hu, C. M. Li, R. Yang, S. E. Kulkova, D. I. Bazhanov, B. Johansson, and L. Vitos, Phys. Rev. B **79**, 144112 (2009).
[58] X. Liang, F. Xiao, X. Jin, T. Fukuda, and T. Kakeshita, Metall. Mater. Trans. A **48**, 2105 (2017).
[59] T. Roy, D. Pandey, and A. Chakrabarti, Phys. Rev. B **93**, 184102 (2016).